Proceedings of the ASME 2017 International Design Engineering Technical Conferences & Computers and Information in Engineering Conference
IDETC/CIE 2017
August 6-9, 2017, Cleveland, Ohio, USA

DETC2017-67841

AN EXPERIMENTAL PARAMETRIC STUDY OF AIR-BASED BATTERY THERMAL MANAGEMENT SYSTEM FOR ELECTRIC VEHICLES

Yuanzhi Liu
Department of Mechanical Engineering
The University of Texas at Dallas
Richardson, Texas 75080, USA
Email: yuanzhi.liu@utdallas.edu

Mao Li
Beijing Institute of Aerospace Testing Technology
The University of Texas at Dallas
Richardson, Texas 75080, USA
Email: limaobuaa@gmail.com

Jie Zhang*
Department of Mechanical Engineering
The University of Texas at Dallas
Richardson, Texas 75080, USA
Email: jiezhang@utdallas.edu

ABSTRACT

This paper develops an experimental platform and performs a parametric study of an air-based battery thermal management system (BTMS) for electric vehicles. A flexible experimental platform with ten battery cells is built up to investigate how key BTMS design parameters affect the battery thermal performance. Three design parameters are studied in this paper, including the mass flow rate of cooling air, the heat flux from the battery cells to the cooling air, and the passage spacing size. To evaluate the thermal performance of the battery system, two metrics (i.e., the maximum temperature rise and the maximum temperature Uniformity) are used. A design of experiments (here 30 groups) are conducted to analyze how the three key design parameters affect the thermal performance of the BTMS. A computational fluid dynamics (CFD) of the BTMS is also performed to compare and help explain the experimental results. Both the experimental and CFD simulation results shows that: (i) decreasing the mass flow rate may deteriorate the thermal performance of the battery module; (ii) increasing the heat flux and enlarging the passage spacing size also deteriorate the battery thermal performance.

Keywords: Battery management, BTMS, thermal performance, design of experiments, electrical vehicles

*Address all correspondence to this author.

1 INTRODUCTION

Lithium-ion batteries are becoming the primary power sources for electric vehicles (EVs) during the past decades. However, the narrow range of the optimum operation temperature is still one of the key issues that restrain their wide use in the electricl vehicle industry [1],[2]. The appropriate operating temperature range should be maintained between 25 °C to 40 °C to yield a better performance. Otherwise, a lower temperature or overheating, in particular, will shorten the cycle life of lithium-ion batteries and even lead to safety issues such as combustion and explosions [3],[4]. Battery thermal management system (BTMS) is accordingly developed to control the temperature. Existing BTMS includes the air-based systems, liquid-based systems, phase change material-based systems, heat pipe-based systems, and hybrid systems [5],[6],[7].

The air-based BTMS has been widely used in EVs due to its advantages such as simple structure, low cost, and light weight. Several methods have been developed in the literature to study the air-based BTMS, such as BTMS modeling, numerical simulations, and experiments. The majority of numerical simulation study are carried out with the computational fluid dynamics (CFD) method. For example, Hwang *et al.* [8] built up an air-based BTMS numerical model using CFD, and found that the location and shape of the air inlet and outlet had significant influences on the temperature distribution and heat dissipation. Park *et al.* [9] simulated the cooling performance employing different manifolds for air ventilation and presented that adding

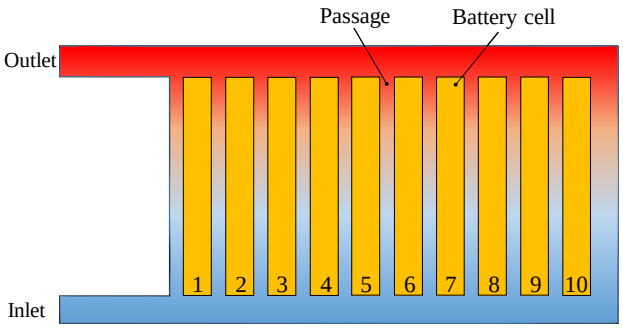

FIGURE 1. The conceptual design of a BTMS experiment system

extra ventilation can effectively improve the cooling performance. Xun *et al.* [10] developed numerical models for BTMS to analyze the impacts of the volume ratio and the spacing size of cooling channel, and found that the battery temperature uniformity and energy efficiency could be reinforced by enlarging the channel size. Sun *et al.* [11] proposed a Z-type air cooling tapered manifold, and CFD simulations showed that this new design can improve the temperature uniformity of the battery pack. Ji *et al.* [12] proposed a temperature control method by optimally arranging the battery cells and controlling the air flow rate to equalize the temperature distribution.

There also exist many studies focusing on experimentations to improve the existing battery module design by analyzing the experimental parameters. For example, Zhao *et al.* [13] established air cooling models for a cylindrical lithium-ion battery pack to study the impacts of different parameters on heat dissipation, such as battery cells passage spacing size, environmental temperature, ventilation type, and battery dimension. Ye *et al.* [14] built an integrated model with heat pipe, fins, and cooling plate, and experiments showed that the integrated model was able to manage twice maximum heat generated from 8 C-rate charging compared to individual models.

However, most of the existing studies have not comprehensively analyzed the impacts of key BTMS design parameters on the thermal control performance, and few experiments were carried out to verify the CFD models. This mutual verification between experiments and numerical simulations could be potentially useful for the optimization of BTMS design. Therefore in this paper, a flexible air-based BTMS experimental platform is established to study the effects of different key design parameters on BTMS design. This paper will mainly investigate the influence of three key parameters, including the mass flow rate of the cooling air, the heat flux on the battery cell wall, and the passage spacing size between adjacent battery cells.

TABLE 1. The setup of experimental parameters

Level	1	2	3	4	5
$\dot{m}$ (g/s)	4.7	5.5	6.3	7.1	7.9
$\dot{q}$ (W/m^2)	220	245	270	295	320
b (mm)	2.0	2.5	3.0	3.5	4.0

2 THE SELECTION OF KEY DESIGN PARAMETERS

The BTMS aims to dissipate the heat generated by the electric vehicles timely. The temperature of the battery module may rise rapidly if the BTMS fails. For an air-based BTMS (Fig. 2), flowing air is used as the heat transfer agent to take away all the heat generated in the battery modules. The heat exchange between the battery cell walls and the cooling air is modeled by the following Eqs. 1 and 2.

$$q = h(T_w - T_a) \tag{1}$$
$$\dot{q} = q/A \tag{2}$$

where q is the heat power, h is the convective heat transfer coefficient, T_a is the temperature of the cooling air near the wall, $\dot{q}$ is the heat flux, A is the area of the battery cell, and T_w is the temperature of the battery cell wall.

Generally, T_w can be regarded as the ambient operating temperature of battery cells. One of the control goals of BTMS is to ensure T_w within an optimal range. After the temperature of the battery module reaches balance, the heat generation is equal to the heat taken away by the cooling air. The correlation between the temperature difference of the cooling air and the heat can be described in Eqs. 3 - 5.

$$q = c_p \dot{m} \Delta T_a \tag{3}$$
$$\Delta T_a = T_{in} - T_{out} \tag{4}$$
$$\dot{m} = \rho v A_f \tag{5}$$

where c_p is the specific heat at a constant pressure, which can be assumed to be constant if the pressure does not change significantl. $\dot{m}$ is the mass flow rate, ρ and v are the density and velocity of the cooling air, respectively. And A_f is the flow area.

Equations (1)-(5) can be used to help set up the initial BTMS parameters before experiments. For example, increasing the flow rate of cooling air can lower the air temperature difference. T_{out} will decrease by increasing the flow rate $\dot{m}$.

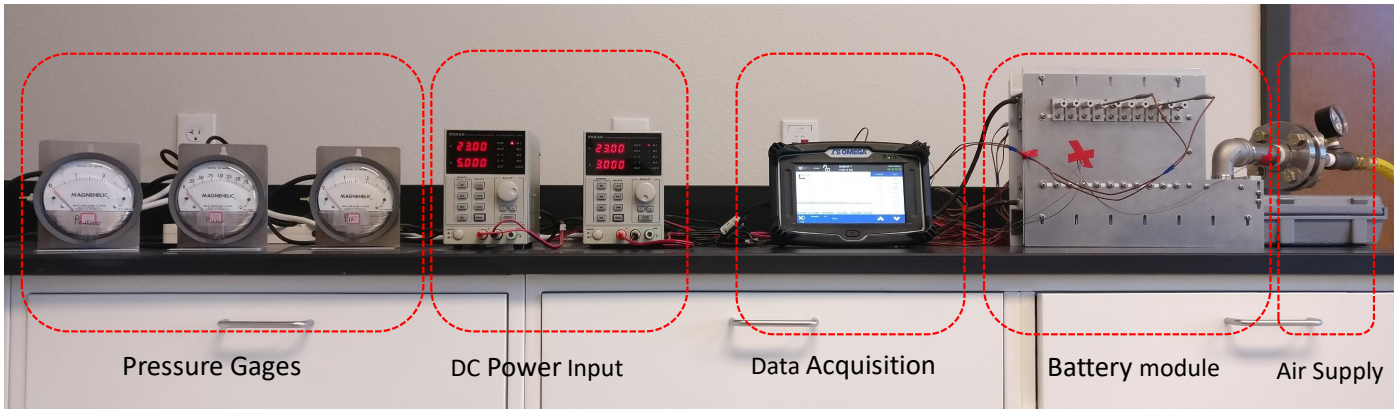

FIGURE 2. The air-based battery thermal management experiment system

To evaluate the BTMS thermal performance, two metrics are introduced in this parametric study, which are the maximum temperature rise and the temperature uniformity in the battery module. A design of experiments (as shown in Table 1) is performed on three selected key parameters, i.e., the mass flow rate of the cooling air ($\dot{m}$), the heat flux of the battery cell wall ($\dot{q}$), and the passage spacing size (b). The design benchmark values of the mass flow rate, heat flux, and passage spacing size are 6.30 g/s, 270 W/m^2, and 3 mm (even size), respectively. The initial parameters of all the experiments in this paper are set to be the benchmark values. The initial ambient temperature is 293 K, maintained by the central air-conditioning. The temperature of the cooling air is also set at 293 K.

3 EXPERIMENTAL PLATFORM DESIGN AND SETUP

Figure 2 shows the air-based battery thermal management experiment system that consists of three main parts: the air supply subsystem, the battery module, and the measurement and data acquisition module.

3.1 Battery Module

The heat generation from the battery cells during charging/discharging varies from different operations. In some extreme testing conditions, the maximum temperature of the battery cells may exceed the allowable range, which may lead to an explosion. For the sake of safety, battery cells made of aluminum are used in our experimental platform to replace the real Lithium-ion batteries. Figure 3 shows the battery module design, in which there are 10 prismatic battery cells (65 mm in length, 151 mm in height, and 16 mm in width). To adapt with different passage spacing sizes, the ten battery cells are fixed on the lateral plate with bolts. In addition, the calculated height of the inlet and outlet

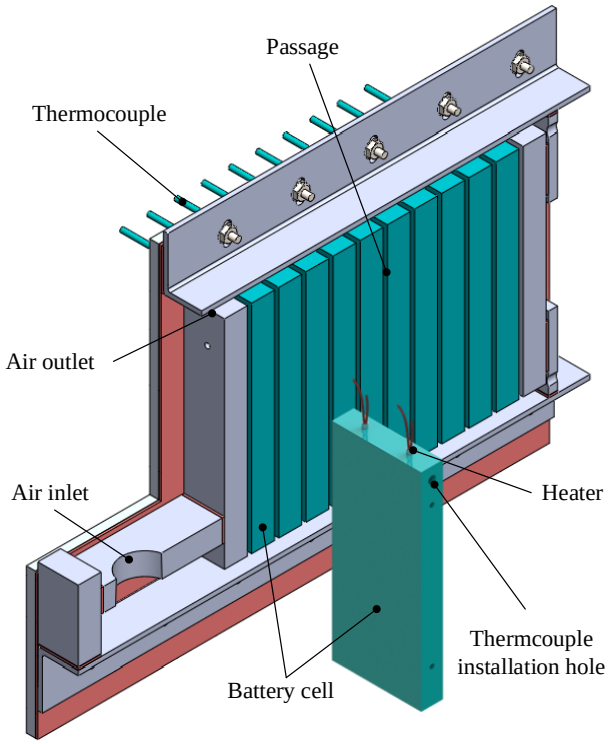

FIGURE 3. The isometric view of the battery cells arrangement

manifold is set to be 6 mm; in order to reduce the impact of electrical wires for heating, the final height is fixed at 8 mm.

Two heaters wrapped with thermal silica are placed evenly in each battery cell to simulate the internal electrochemical heat generated during the charging and discharging process. The heat flux of the battery model ranges from 220 W/m^2 to 320 W/m^2, which is supplied by two ad-

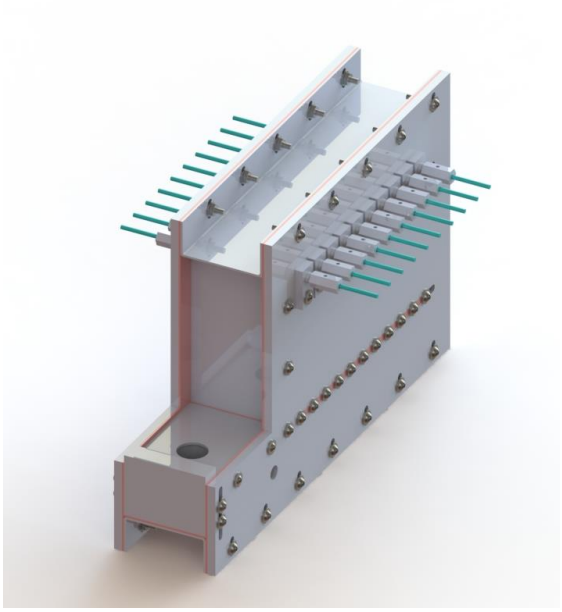

(a) The battery module renderings

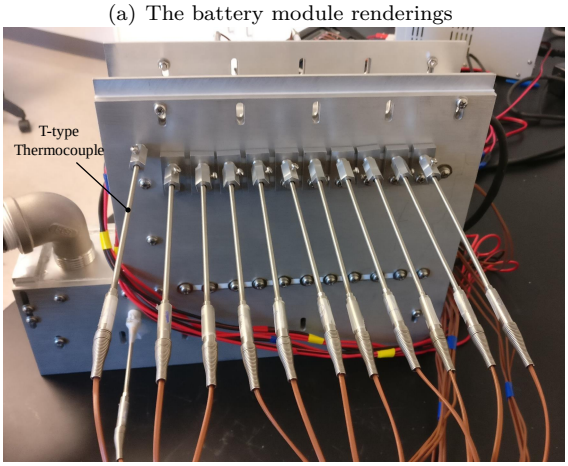

(b) The battery module with thermocouples

FIGURE 4. Schematic model of the battery module

justable DC power sources. The heat flux range is set to be equal to that of real battery cells under different charging rates. Teflon plates are utilized for the purpose of sealing and thermal insulation. Figures 3 and 4 illustrate more details of the battery module.

3.2 The Air Supply Subsystem

A stable compressed air source with 50 psi is used to supply the cooling air. To control the mass flow rate of the cooling air, a pore plate is applied. The mass flow rate can be determined using Eq. 6

$$\dot{m} = C_d K \frac{p^*}{\sqrt{T^*}} A \tag{6}$$

Where $\dot{m}$ is the mass flow rate, C_d is the flow coefficient (C_d equals to 1.0 when the fluid is non-viscous, and it is set to be 0.7 here), K is a constant (for air, K equals to 0.0404), p^* is the total pressure, T^* is the total temperature, and A is the area of the pore. Equation 6 can be used only when the air flow in the pore reaches the speed of sound. Thus, the pressure ratio between the downstream and the upstream of the pore plate should be smaller than 0.54. This prerequisite is satisfied in this experiment. The experiment paltform is designed in a flexible manner, and different mass flow rates can be obtained by replacing the pore plate with a different diameter.

3.3 Measurement and Data Acquisition Module

In the experimental system, a total of 14 T-type Omega thermocouples with an accuracy of ± 0.1 K are inserted into the top of battery cells to monitor the interior temperature. The position is considered as the hottest point since cooling air flows from bottom to top. The temperature data are collected and stored at a sampling frequency of 12 per minute. Besides the maximum temperature of every battery cell after air cooling, the initial temperature before experiments is also measured, which is used as a baseline temperature to calculate the temperature increase.

The pressure drop is another important parameter in the BTMS. The cooling air is supplied by a stable compressed air source in the experiment, while it is provided by a fan in actual EV application. The relationship among the fan power, efficiency, pressure difference, and volume flow rate is described as follows.

$$P = \Delta p \dot{V} / \eta \tag{7}$$

where P is the power of the fan, Δp is the pressure difference between the inlet and outlet, $\dot{V}$ is the volume flow rate through the fan, and η is the efficiency.

It is seen from Eq. 7 that a larger Δp will decrease $\dot{V}$ as the power input remains constant, which deteriorates the cooling performance. For a certain battery module, increasing the volume flow rate $\dot{V}$ will also increase the pressure difference Δp and finally generates a larger P, which will consume more energy from the battery. Moreover, a fan of larger power generally requires more installation space. We use three pressure difference gauges to obtain the pressure in our experiemnts.

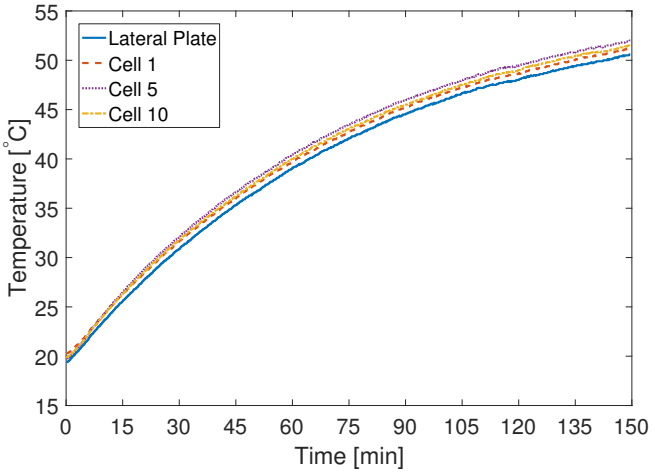

FIGURE 5. The temperature rise of battery module without any forced air ventilation

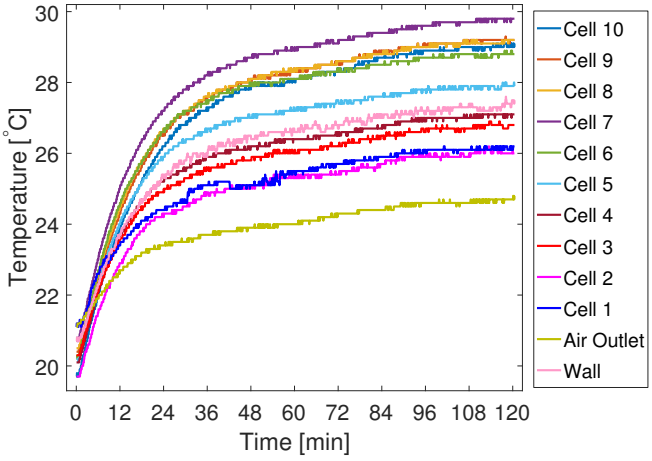

FIGURE 6. The dynamical process of the temperature rise

4 RESULT AND DISCUSSION

4.1 Air-based BTMS Dynamics Process Analysis

Figure 5 shows the temperature rise of the battery module without any forced air ventilation. Since the battery model is made of aluminum, there is no need to take the safety issues into consideration, and thus temperature that are higher than the critical safety point can be obtained. As seen in Fig. 5, the temperature increases rapidly in two hours, and the highest temperature of battery model surface has exceeded 50°C. The temperature increasing rate of the ten battery cells is almost the same, which implies that the effect of natural air convection for battery dissipation is negligible. And the maximum temperature is determined only by the heater's input power and the heating duration. Studies have shown that a high temperature will significantly shorten the long-scale life and reduce the battery capacity. The lithium-ion battery would likely to lose 70% of initial storage capacity after 500 cycles at 55°C and 60% of initial storage capacity after 800 cycles at 50°C [15],[16],[17]. The temperature of the lateral plate has also reached 50°C. The temperature rising rate decreases after the temperature reaches 40°C. This is due to that the radiative and convective heat transfer between the aluminum lateral plate and the ambient air is strengthened, though a 1.6 mm Teflon plate is stuck to the aluminum plate as a thermal isolation.

The dynamics ascending process of the BTMS model temperature is shown in Fig. 6. The mass flow rate of cooling air is 7.1 g/s, and other parameters are the same as the experiment without any cooling ventilation. The temperature increases rapidly at the beginning and then in a relatively slight rate after 25 minutes. The convective heat transfer is strengthened due to a higher temperature difference between the battery cell and the cooling air. The whole system achieves the thermal dynamics balance in approximately 90 minutes. Detailed properties of the thermal dynamics will be discussed in the next three subsections.

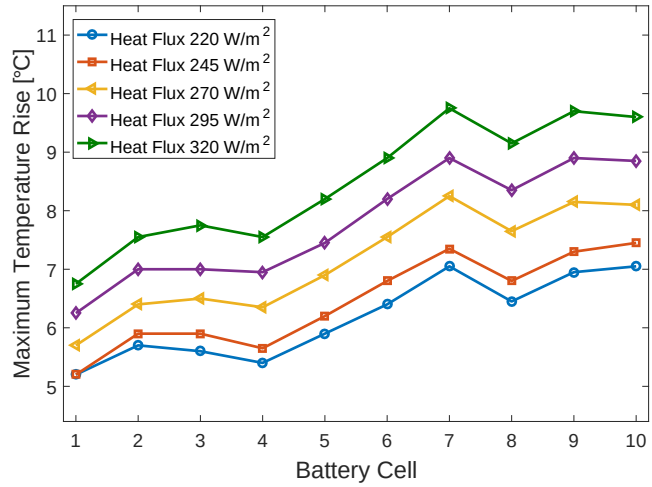

FIGURE 7. Effects of heat flux on the maximum temperature rise

4.2 Effects of The Heating Flux

Figure 7 shows the temperature differences of five levels' heat flux for each battery cell. The initial temperatures of the battery cells have a deviation within 1 K, so only the temperature rising curves are presented. The five curves, as well as the curves in Figs. 8 and 9 of the following subsection, share a similar linear tendency. Note that the model is U-type, and the pressure drops of the front channels (i,e., close to the air inlet) are more than those of the rear ones. Thus more cooling air outflows through the front channels, taking more heat away from the battery module. The max-

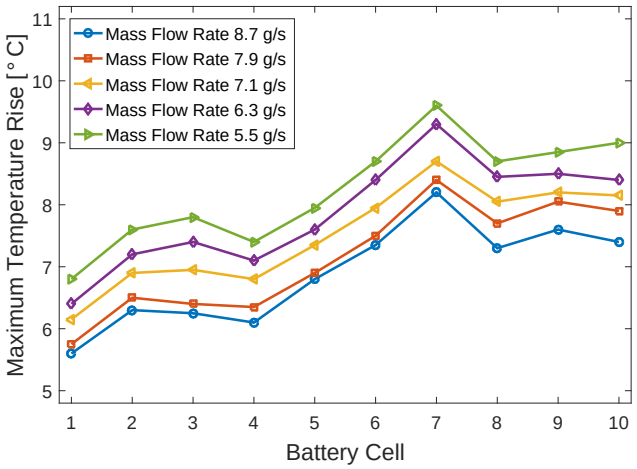

FIGURE 8. Effects of the mass flow rate on the maximum temperature rise on the battery cells

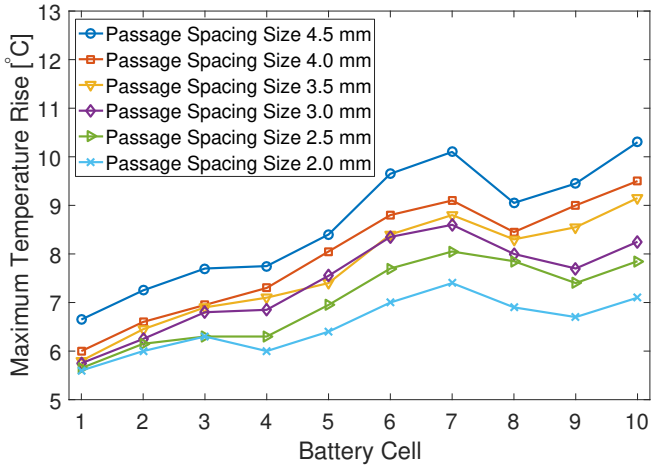

FIGURE 9. Effects of the passage spacing size on the maximum temperature rise

imum temperature rise increases successively from the air inlet to the rear side. It is seen that the peak temperature rise occurs at the seventh cell. This will be further explained in the following CFD analysis subsection.

As the heat flux increases from 220 W/m^2 to 320 W/m^2, the maximum temperature rise of the battery cell near the inlet only increases from 5.2 K to 6.8 K, while that of the rear one increases approximately from 7 K to 10 K. Also, the temperature uniformity of the 220 W/m^2 case at the thermal dynamics balance point is 1.5 K, compared to the 3 K of the 320 W/m^2 case. Overall, the temperature uniformity becomes more uneven with the increase of heat flux. Both the phenomena above illustrate that a higher heat flux will significantly deteriorate the thermal dissipation performance of the rear battery cells with the U-type model. Other types of models (e.g., Z-type) will be studied in the future.

4.3 Effects of The Mass Flow Rate

Figure 8 shows the effects of the cooling air mass flow rate on the maximum temperature rise. It is seen that, as the cooling air mass flow rate increases from 5.5 g/s to 8.7 g/s, the maximum temperatures of the front and the rear battery cells decrease from 7 K to 5.5 K and 9 K to 7 K, respectively. The temperature uniformity decreases from 2 K to 1.5 K, indicating that a larger mass flow rate would equalize the temperature distribution within the battery module. In contrast, the pressure of the air inlet increases from 290 Pa to 525 Pa. In the actual EV system, where a fan is used to supply the cooling air, a larger pressure difference between the inlet and the outlet causes more power consumption. Moreover, A larger fan would occupy more space that could be used for battery cell installation. Thus, it's an inferior strategy to improve the thermal performance merely by increasing the mass flow rate. Further research needs to be performed to optimize the balance between the temperature rise and the pressure drop.

4.4 Effects of The Passage Spacing Size

Figure 9 presents the effects of different passage sizes on the thermal performance. As the passage spacing size becomes larger, the temperature of rear battery cells increases at a much greater rate than the front ones. The temperature rise at the tenth battery cell reaches 10 K at the passage spacing of 3 mm, compared to 7 K at the passage spacing of 2 mm. A larger spacing size will worsen the thermal dissipation of rear ones. The temperature uniformity also change approximately from 1.5 K to 4 K. It may suggest that the thermal performance of smaller passage size is better, yet noting that a narrow cooling channel may cause a bigger pressure drop. According to Eq. 7, as the mass flow rate remains constant, more energy will be consumed.

4.5 CFD Analysis

For the peak temperature rise value at the seventh battery cell, repeated tests are carried out to eliminate the possibilities of assembly errors, heater fault, and thermocouple inaccuracy. The speed and pressure drop of every channel have gone beyond the experiment's measurability.

In order to further explain this phenomenon, a CFD air-based BTMS model is built using the commercial software ANSYS Fluent. The passage spacing size is set at 3 mm; the heat flux of the battery call wall is 245 W/m^2; the mass flow rate is 6.3 g/s. The boundary condition of air inlet is

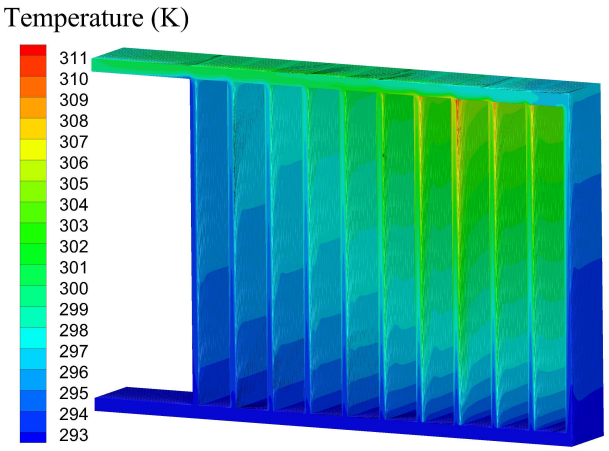

FIGURE 10. The temperature distribution of the cooling air in BTMS

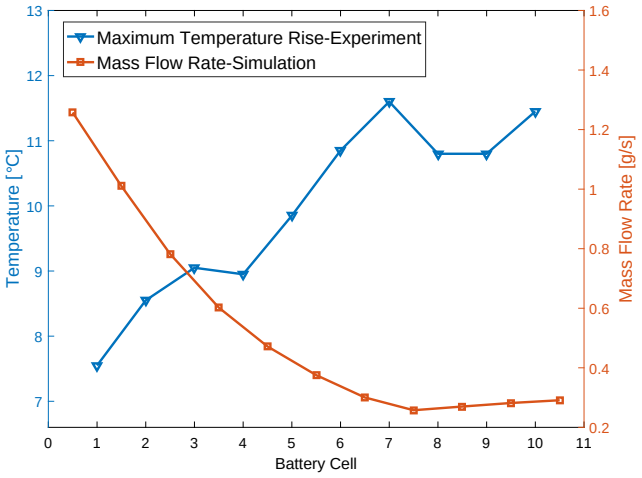

FIGURE 11. The battery maximum temperature rise, corresponding to the left Y axis; the mass flow rate, corresponding to the right Y axis.

set to be mass flow rate inlet, and air outlet is set to be pressure outlet. The properties of the battery cell walls are with heat flux, while the battery module walls are adiabatic and no-slip. The SIMPLEC method and the transition SST turbulence model are selected to analyze this model. The thermal radiation transfer is assumed to be negligible in this simulation.

Figure 10 shows the simulation results of temperature distribution in this battery module. The highest simulated temperature of cooling air occurs at the eighth passage, which is next to the maximum temperature rise battery cell (seventh). The mass flow rate distribution of the passages is presented in Fig. 11. It is seen that the mass flow rate of the eighth passage is only 0.25 g/s, which is the lowest and approximately one-sixth of that in the first channel. The Reynolds number of the passages changes from 1,306 to 267, sharing the same changing pattern as the mass flow rate. Since the Reynolds number is below 2,040, the cooling air flows in all passages are laminar flow, implying the same convective heat transfer coefficient. According to Eqs. 1 - 5, the temperature of the battery cells is highly correlated with the passage mass flow rate. This is why the highest temperature rise occurs at the seventh battery cell. The temperatures of the rear battery cells are also higher that the front ones.

5 CONCLUSION

This paper performed a parametric study of an air-based battery thermal management system (BTMS) in electric vehicles. A number of interesting observations were obtained by analyzing the effects of three key BTMS design parameters on the battery thermal performance.

1. Under the situations without any air cooling ventilation, the battery module was heated up close to the acceptable safety temperature in 2 hours.
2. The dynamic process of the cooling system reached the steady state in 90 minutes.
3. Increasing the mass flow rate could reduce the maximum temperature rise and improve the temperature uniformity. But, it is not an ideal strategy, since more energy will be consumed by increasing the mass flow rate.
4. A larger heat flux may result in a higher maximum temperature rise and a more nonuniform temperature distribution. A larger spacing size acts in a same manner.

Based on the analysis above, reducing the mass flow rate of the front battery passages and increasing the mass flow rate of the rear ones, may contribute to the temperature uniformity of the battery module. This can be achieved by rearranging the spacing size of each passage through an optimization strategy. For the future work, we will continue to investigate the effects of tapered inlet/outlet manifold, Z-type BTMS, and rearrange the battery passage spacing size by experiments.

6 ACKNOWLEDGEMENT

This work is supported by the University of Texas at Dallas. The author of Mao Li is supported by the China Scholarship Council.

REFERENCES

[1] Kizilel, R., Sabbah, R., Selman, J. R., and Al-Hallaj, S., 2009. "An alternative cooling system to enhance the safety of li-ion battery packs". *Journal of Power Sources,* ***194***(2), pp. 1105–1112.

[2] Rao, Z., and Wang, S., 2011. "A review of power battery thermal energy management". *Renewable and Sustainable Energy Reviews,* ***15***(9), pp. 4554–4571.

[3] Bandhauer, T. M., Garimella, S., and Fuller, T. F., 2011. "A critical review of thermal issues in lithium-ion batteries". *Journal of the Electrochemical Society,* ***158***(3), pp. R1–R25.

[4] Pesaran, A. A., 2002. "Battery thermal models for hybrid vehicle simulations". *Journal of Power Sources,* ***110***(2), pp. 377–382.

[5] Jarrett, A., and Kim, I. Y., 2014. "Influence of operating conditions on the optimum design of electric vehicle battery cooling plates". *Journal of Power Sources,* ***245***, pp. 644–655.

[6] Fan, L., Khodadadi, J., and Pesaran, A., 2013. "A parametric study on thermal management of an air-cooled lithium-ion battery module for plug-in hybrid electric vehicles". *Journal of Power Sources,* ***238***, pp. 301–312.

[7] Choi, Y. S., and Kang, D. M., 2014. "Prediction of thermal behaviors of an air-cooled lithium-ion battery system for hybrid electric vehicles". *Journal of Power Sources,* ***270***, pp. 273–280.

[8] Hwang, H.-Y., Chen, Y.-S., and Chen, J.-S., 2015. "Optimizing the heat dissipation of an electric vehicle battery pack". *Advances in Mechanical Engineering,* ***7***(1), p. 204131.

[9] Park, H., et al., 2013. "A design of air flow configuration for cooling lithium ion battery in hybrid electric vehicles". *Journal of Power Sources,* ***239***, pp. 30–36.

[10] Xun, J., Liu, R., and Jiao, K., 2013. "Numerical and analytical modeling of lithium ion battery thermal behaviors with different cooling designs". *Journal of Power Sources,* ***233***, pp. 47–61.

[11] Sun, H., and Dixon, R., 2014. "Development of cooling strategy for an air cooled lithium-ion battery pack". *Journal of Power Sources,* ***272***, pp. 404–414.

[12] Ji, B., Song, X., Cao, W., and Pickert, V., 2013. "Active temperature control of li-ion batteries in electric vehicles". *Hybrid and Electric Vehicles Conference 2013 (HEVC 2013), IET*, pp. 1–5.

[13] Zhao, J., Rao, Z., Huo, Y., Liu, X., and Li, Y., 2015. "Thermal management of cylindrical power battery module for extending the life of new energy electric vehicles". *Applied Thermal Engineering,* ***85***, pp. 33–43.

[14] Ye, Y., Shi, Y., Saw, L. H., and Tay, A. A., 2016. "Performance assessment and optimization of a heat pipe thermal management system for fast charging lithium ion battery packs". *International Journal of Heat and Mass Transfer,* ***92***, pp. 893–903.

[15] Lu, L., Han, X., Li, J., Hua, J., and Ouyang, M., 2013. "A review on the key issues for lithium-ion battery management in electric vehicles". *Journal of Power Sources,* ***226***, pp. 272–288.

[16] Ramadass, P., Haran, B., White, R., and Popov, B. N., 2002. "Capacity fade of sony 18650 cells cycled at elevated temperatures: Part i. cycling performance". *Journal of Power Sources,* ***112***(2), pp. 606–613.

[17] Ning, G., Haran, B., and Popov, B. N., 2003. "Capacity fade study of lithium-ion batteries cycled at high discharge rates". *Journal of Power Sources,* ***117***(1), pp. 160–169.